5-2019

Light Addressable Electrode for Neurotransmitter Sensing

Irina Michelle Terrero Rodríguez
Montclair State University

Abstract

Electrochemical sensors are important for a variety of applications. However, they suffer from physical constraints, as each electrode requires a dedicated wire. Although arrays of 500 electrodes have been reported, achieving high-density electrochemical measurements is still difficult.

In a light-addressable electrode, electrochemical processes occur only when the electrode is illuminated. Light-addressable electrodes could potentially solve many of the drawbacks of traditional electrode arrays, as light is used to spatially confine the redox process to only a small part of the electrode and only one connection is needed. It could also allow for new imaging techniques.

Light-addressable electrodes require a semiconductor layer, often Si, with one or more protective layers. A spontaneous SiO_x layer forms when Si comes into contact with oxygen or water, so a protective layer is required to prevent Si from degrading in aqueous media while facilitating the reaction. The semi conductive nature of Si allows the redox reaction to be controlled by light, as Si has a relatively small bandgap and electrons can jump from the valence band to the conducting band when provided with an extra energy input.

We show the fabrication and characterizations of light-addressable electrodes that are simple to produce, inexpensive and scalable. Moreover, the method does not require clean room techniques or a passivating organic self-assembled monolayer. Instead, we protect the underlying Si layer with electrodeposited Au nanoparticles. We fabricate the electrodes using a two-step method and characterize them in catechol, dopamine and ferrocene methanol using three illumination conditions (Overall illumination, local illumination and no illumination). Briefly,

we prepare a n-type Si electrode and remove the native SiO_x layer by etching in 40% NH_4F and then electrodeposit Au nanoparticles for 20 minutes. The electrodes are characterized using SEM-EDS imaging, cyclic voltammetry and chronoamperometry.

When a voltage is applied under no illumination conditions, the electrode does not pass significant current. However, when the whole electrode surface is illuminated, enough carriers are generated to observe a redox event and the peak current increases roughly two orders of magnitude. When only a small part of the electrode is illuminated, the current density is roughly one order of magnitude lower than when overall illumination is used. For a simple redox event, peak current is directly proportional to electrode area.

The electrodes are stable in aqueous solution for 1000 consecutive cycles. Dopamine and catechol calibration curves with excellent linearity were obtained using total illumination, dopamine. These results pave the way for future experiments, such as measuring dopamine release by a cell.

MONTCLAIR STATE UNIVERSITY

Light-Addressable Electrode for Neurotransmitter Sensing

by

Irina M. Terrero Rodríguez

A Master's Thesis Submitted to the Faculty of

Montclair State University

In Partial Fulfillment of the Requirements

For the Degree of

Master of Science

May 2019

College of Science and Mathematics

Department of Chemistry and Biochemistry

Thesis Committee:

[redacted]

Prof. Glen D. O'Neil
Thesis Sponsor

[redacted]

Dr. Lynn F. Schneemeyer
Committee Member

[redacted]

Dr. David Talaga
Committee Member

LIGHT ADDRESSABLE ELECTRODE FOR NEUROTRANSMITTER SENSING

A THESIS

Submitted in partial fulfillment of the requirements

For the degree of Master of Science

by

IRINA MICHELLE TERRERO RODRÍGUEZ

Montclair State University

Montclair, NJ

2019

Acknowledgments

I would like to begin by thanking my thesis sponsor, Prof. O'Neil, for letting me work in this project. He was patient (and kind!) enough to answer my dumb questions without making me feel dumb. I learned so much about semiconductor electrochemistry, data analysis, formatting, writing and presentation slides. Your encouragement and guidance have been priceless, and I am so happy to have worked in such a nurturing environment. I would also like to acknowledge my lab mates in the O'Neil group: Jordyn, Shakir, Alex, John, Kelly, Kevin and Alexa. It has been a pleasure running experiments and analyzing data next to you. 10/10, would recommend as a lab group. I would like to thank the students, faculty and staff in the Department of Chemistry and Biochemistry at Montclair State University.

Many thanks to my parents, Yris and David, for believing in me. Your continued interest in my education has made me the person I am today. I would not have made it this far without your love and encouragement. I guess I should also thank my brothers, David A. and Abel, for always reminding me that I got lucky because I got to study abroad. Special thanks to Abel for being my concert buddy. I would also like to acknowledge my friends, aunts, uncles, cousins and grandparents in the Dominican Republic, for all the love and support. You know who you are! It means a lot to me to know you are proud of my endeavors, even if no one has ever asked me what my research is in. Thank you Shantal for all the memes you sent me. They made me laugh during very stressful times.

I want to thank the friends I made at Montclair State: Yosalen, Ananír, Valerie. You gracefully listened to me complain for the last two years. Many thanks to my Utah State University friends: Iván, Laysa, Elaine, Nathalie and Mallory, who have been listening to me

complain for the past six years. You made moving to NJ easier, and I am thankful for friendships that last through the distance.

Last, I would like to thank my fiancé, Mario, for the encouragement, for patiently listening to all of my practice talks and for giving me invaluable input. You are my biggest fan and I am lucky to have you. All the clichés are true. Te amo mucho mucho muchísimo. ¡Gracias totales!

Table of Contents

List of Figures

2 Theory and Background

Electrochemical sensors offer many benefits: they are selective, sensitive, and do not require a label or expensive instrumentation. However, the number of measurements that can be collected in a given area (measurement density) is spatially limited because each electrode requires an individual connection to the potentiostat.[1] As a result, electrochemical sensing methods have not reached the measurement density of optical methods, which offer up to 10^5 simultaneous measurements.[2,3] Increasing measurement density would provide electrochemical methods with better statistical power, high spatial resolution, smaller sensor footprint, and the ability to multiplex.

Low measurement density is partially solved by using individually addressable electrode arrays, which can collect ~10^3 measurements simultaneously.[2–4] Electrode arrays are also used in electrochemical imaging techniques, but there are blind spots in the spaces between the electrodes (Figure 1A).[2–4] This problem could be avoided by using scanning electrochemical microscopy (SECM), which uses an ultramicroelectrode (UME) scanning tip that is moved to probe an electrochemically active surface.[5–8] However, these measurements have long sampling times, which makes this technique unsuitable for applications that require fast data collection.[5–8]

One alternative approach is to use a light-addressable electrode as an electrochemical sensor. In a light-addressable electrode, electrochemical processes occur only where the electrode is illuminated (Figure 1B).[1] Light-addressable electrodes could potentially solve the slow sampling times of SECM and the complicated wiring of traditional electrode arrays. They require only one electrical connection because focusing the light on a single spot creates a transient electrode. Moving a light source across the surface of the electrode makes sampling times faster and reduces the physical constraints on measurement density. In addition, this type of electrode could allow for

easily modifiable arrays without predetermined geometries and for electrochemical imaging with shorter sampling times.

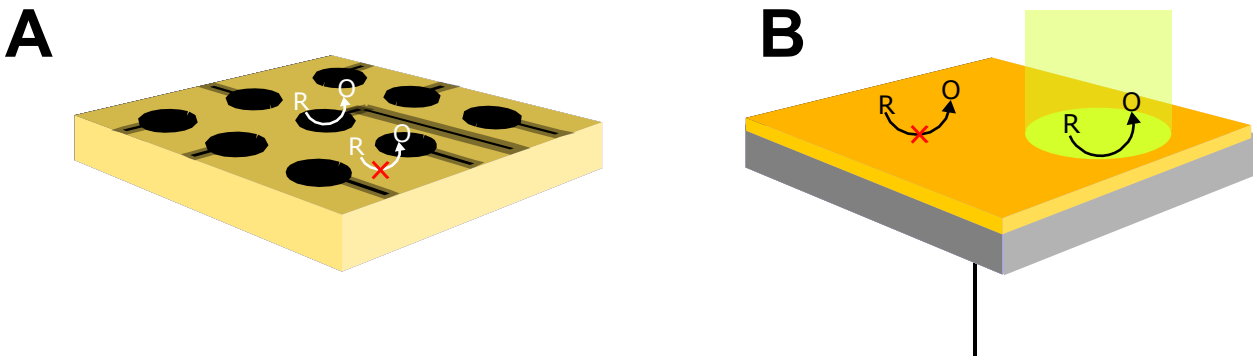

Figure 1. Comparison between (A) individually addressable electrode array and (B) Light-addressable electrode, where electrochemical processses occur only where the electrode is illuminated.

Light-addressable electrodes require a semiconductor layer, often Si, with one or more protective layers.[1] An insulating SiO_x layer forms spontaneously when Si comes into contact with oxygen or water, so a protective layer is required to prevent Si from degrading in aqueous media while facilitating the reaction.[1] The semiconductive nature of Si makes the redox reaction controlled by light, as Si has a relatively small bandgap and electrons can jump from the valence band to the conducting band when provided with photons.[9]

A light-addressable electrode that functions in aqueous solution could prove a powerful technique to probe biological processes. This thesis will describe the fabrication and characterization of light-addressable electrodes for neurotransmitter sensing. We use a simple two-step process where we remove the native SiO_x and then immediately electrodeposit Au nanoparticles. This chapter will provide the necessary scope for understanding electrochemical processes, electroanalytical methods and the basic principles of semiconductor electrochemistry.

2.1 Background and Motivation

Neurotransmitters are signaling molecules secreted by neurons to relay messages to other cells.[10,11] They modulate a myriad of processes, such as organ function, appetite, sleep, muscle contraction and emotional response. Electrochemical techniques have been central to the understanding of how neurons secrete neurotransmitters, the characterization of the chemical properties of neurotransmitters and *in vivo* visualization of how neurotransmitters modify behavior in animals.

Dopamine, a neurotransmitter, is a major component of the brain's reward system (Figure 2A).[10] Alongside norepinephrine and epinephrine, dopamine belongs to the catecholamine neurotransmitter group. Catecholamines possess a benzene with two adjacent hydroxyl groups (catechol) and an amine side-chain (Figure 2B). The catechol moiety is redox active, and both hydroxyl groups can be oxidized to carbonyl groups (Figure 2C). Thus, catecholamines can be studied using electrochemical methods.

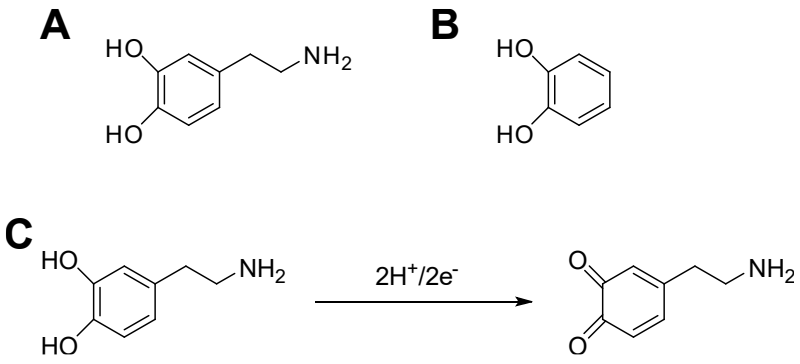

Figure 2. (A) Dopamine. (B) Catechol (C) Dopamine oxidation into dopamine O-quinone.

Neurotransmitter secretion occurs through exocytosis, an energy-dependent process in which a small vesicle that contains neurotransmitters is transported from the inside of the cell to the cell membrane.[10] As the vesicle fuses with the plasma membrane, neurotransmitters are released into the extracellular environment. Dopamine sensing systems require high spatiotemporal resolution,

as exocytosis is a fast process (≈10 ms), the dimension of a cell is on the order of 10 μm and the dopamine concentration in the vicinity of neurons must be measured before it diffuses to the bulk solution or is bound to the receptors of another cell. They must also be able to detect dopamine at very low concentrations, as the concentration of dopamine immediately after exocytosis is in the nM range.

Recently, the Gooding group have fabricated light-addressable electrodes by protecting Si with a monolayer of 1,8-nonadiyine.[1,9,12–14] Functional groups such as ferrocene and Au NPS can be attached to the diene layer, and these aid in the sensing of many different molecules and cellular processes. Gooding's group has characterized charge transfer between semiconductor and solution, in addition to DNA sensing, detection and imaging of K^+ in live cells, and selective cell capture and release. Gooding's Si photoelectrodes have been shown to be stable for hundreds of cycles. However, they require a lengthy synthesis process and clean room techniques. The Chung group fabricated and tested light-addressable electrodes by depositing hematite into fluorine-doped tin oxide (FTO).[15] Although considerably less robust than Gooding's electrodes, Chung's photoelectrodes can be used for several cycles and show promise for dopamine detection.[15]

To our knowledge, there are only two other groups developing this type of electrode. The lack of many examples in the literature coupled with its advantages over traditional electrochemical methods makes light-addressable electrodes an exciting developing field.

2.2 Electrochemical reactions

Electrochemical reactions occur through the transfer of electrons between chemical species.[16,17] The species that loses the electron is said to have been oxidized, whereas the species that gains the electron has reduced. In an oxidation-reduction reaction, there must always be a

chemical species that loses an electron and another species that gains the lost electron. A distinct potential that is related to free energy is associated with each half-reaction.

2.2.1 Nernst equation

The Nernst equation governs the concentration of an electrochemically active species at an applied potential E relative to the formal potential $E^{0'}$, which is the reduction potential of an electroactive species under non-standard conditions.

$$E = E^{0\prime} + \frac{RT}{nF} ln \frac{C_O}{C_R} \quad (1)$$

F is Faraday's constant, n is the number of electrons transferred in the reaction, R is the ideal gas constant and T is temperature. Electrochemical systems that follow the Nernst equation are known as reversible, or Nernstian.[16,17] In a Nernstian reaction, the electron transfer kinetics must be fast so that the concentrations of the oxidized and reduced species in contact with the electrode (C_O and C_R, respectively) are at equilibrium with the electrode potential.

2.2.2 Heterogeneous electron transfer

Faradaic processes involve the transfer of charge across an electrode/solution junction and follow Faraday's law, which relates charge (Q) to the reaction of 1 mole of substance.[16,17]

$$Q = n F \quad (2)$$

Some processes, such as adsorption, double layer charging, and desorption, can also occur when a potential is applied, even when there is no charge transfer. These processes are known as non-Faradaic and must be taken into account when analyzing faradic processes because they affect current flow.

Charge transfer between an electrode and an analyte in solution can occur through two main mechanisms. In an outer-sphere electron-transfer reaction, the reactant and product interact weakly with the electrode surface, as there is at least one solvent layer between the electroactive species and the electrode.[17] In contrast, inner-sphere electrode reactions present strong interactions between the electroactive species and the electrode, usually through adsorption.

2.3 Electrochemical measurements

2.3.1 Electrochemical cell

In the simplest electrochemical cell, two electrical conductors (electrodes) are separated by a conducting solution (electrolyte) and charge is transferred throughout multiple interfaces.[16,17] The electrodes donate or accept electrons, and the electrolyte contacts them through the conduction of ions. An electrochemical half-reaction happens at each electrode interface, and their sum describes the overall process occurring in the electrochemical cell. For analytical purposes, usually only one of the half-reactions is of interest, and the other is fixed. The electrode at which the half-reaction of interest occurs is named the working electrode. The other electrode serves as a reference and maintains a constant potential, so any change in the cell is caused by the working electrode. The potential of the working electrode is often manipulated to probe an analyte present in the electrolyte.[16,17] This is achieved by connecting an external power supply to the cell, which can then increase or decrease the potential of the working electrode.[17] When the potential of the working electrode is higher than the LUMO of the analyte, an electron will be transferred to the analyte (Figure 3). Conversely, when the potential of the working electrode is lower than the analyte's HOMO, the analyte will transfer an electron to the electrode.

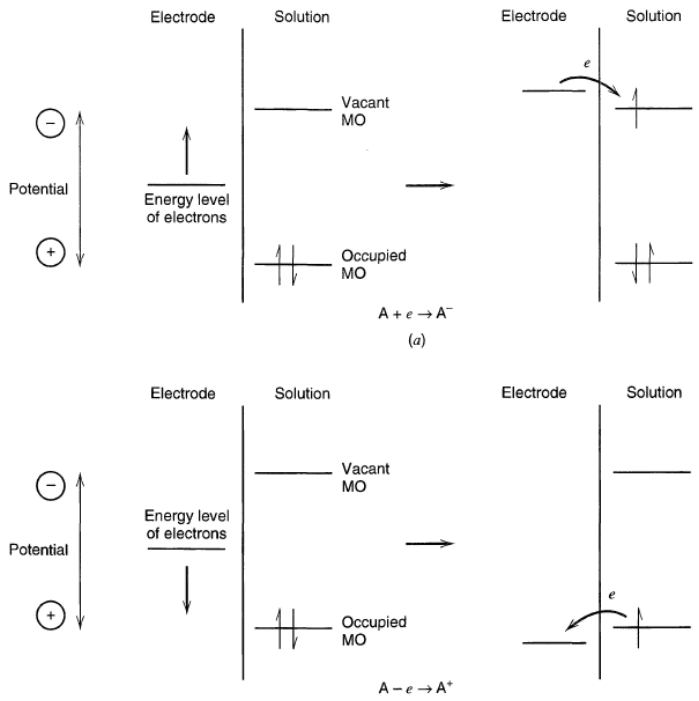

Figure 3. MO diagram showing electrode transfer between electrode and analyte. Taken from Bard, A. J.; Faulkner, L. R. *Electrochemical Methods Fundamentals and Applications*, 2nd ed.; John Wiley & Sons, 2001.

Figure 4 depicts a three-electrode arrangement, which is commonly used to make electrochemical measurements. In a three-electrode arrangement, in addition to the working and reference electrodes, an extra electrode termed the auxiliary or counter electrode is introduced to complete the circuit. [16,17] The counter electrode prevents large currents from passing through the reference electrode and altering its potential.[18] Half-reactions can also occur at the counter electrode, so the surface area of the counter electrode must be higher than that of the working electrode to prevent the kinetics of the side reactions from interfering with the target reaction. A counter electrode is not necessary when the currents generated by the working electrode are very small.

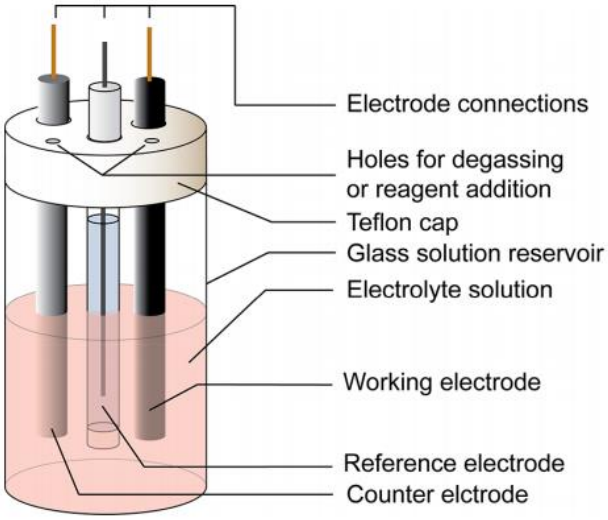

Figure 4. Three-electrode arrangement commonly used to make electroanalytical measuemrents. Taken from Elgrishi, N.; Rountree, K. J.; McCarthy, B. D.; Rountree, E. S.; Eisenhart, T. T.; Dempsey, J. L. A Practical Beginner's Guide to Cyclic Voltammetry. *J. Chem. Educ.* **2018**, *95* (2), 197–206.

2.3.2 Mass transport

Movement of the analyte from the bulk solution to the electrode can occur through three modes:

- Convection: transport of material to the electrode by movement of the solution or the electrode
- Migration: movement of charged species caused by an electrical field
- Diffusion: movement caused by a chemical potential gradient.

The Nernst-Planck equation describes mass transport to an electrode surface. For one-dimensional mass transfer in one direction, the equation becomes

$$J_i(x) = -D_i \frac{\partial C_i(x)}{\partial x} - \frac{z_i F}{RT} D_i C_i \frac{\partial \phi(x)}{\partial x} + C_i v(x) \quad (3)$$

where $J_i(x)$ is flux of species as a function of distance x from the surface, D_i is the diffusion coefficient, $\frac{\partial C_i(x)}{\partial x}$ is the concentration gradient as a function of distance x, $\frac{\partial \phi(x)}{\partial x}$ is the potential

gradient, z_i is the charge, C_i is the concentration and v(x) is the velocity at which the volume moves in the x direction. Each term of the Nernst-Planck equation describes the contribution of one mode of mass transport to the flux: $-D_i \frac{\partial C_i(x)}{\partial x}$ is diffusion, $\frac{z_i F}{RT} D_i C_i \frac{\partial \phi(x)}{\partial x}$ is migration and $C_i v(x)$ is convection.

In order to easily relate current to analyte concentration, diffusion is often isolated as the principal mode of mass transport. To mitigate effects caused by migration and convection, the solution is not stirred and an inert electrolyte in a much higher concentration than the analyte is added. As the electrochemical reaction proceeds, the reactant concentration around the electrode decreases, and a concentration gradient is established around the electrode, which allows the analyte to diffuse to the electrode.

There are two types of diffusional fields: linear and hemispherical (Figure 5). Planar electrodes with size >25 μm tend to have linear diffusional fields.[16] However, for planar electrodes with a radius in the μm range, the diffusional field is hemispherical at typical scan rates. This gives rise to unique mass transport properties, which are exploited by ultramicroelectrodes (UMEs).

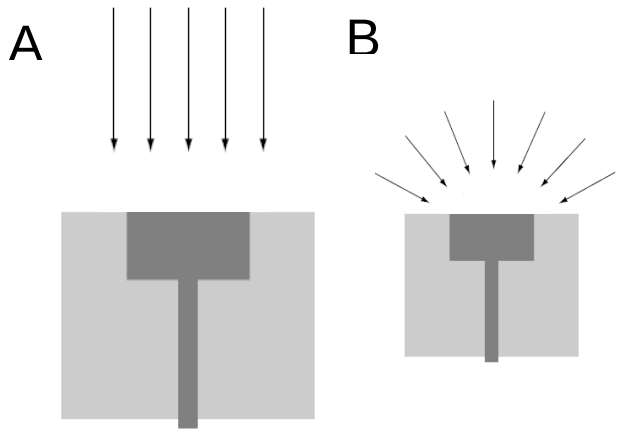

Figure 5. Linear (A) and hemispherical (B) difussional fields in planar electrodes. From: Wang, J. *Analytical Electrochemistry*, 2nd ed.; Wiley-VCH, 2000.

2.3.3 Electron transfer kinetics

In electrochemical systems, current is a measure of the rate at which electrodes are transferred between the electrode and the analyte. The Butler-Volmer equation governs electron transfer-limited reactions and relates current to the overpotential ($E-E^0$), heterogeneous rate constant ($k°$), the transfer coefficient (α) and the concentrations of oxidized and reduced analyte (C_O and C_R, respectively).

$$i = nFAk° \left(C_O e^{\frac{-\alpha nF(E-E°)}{RT}} - C_R e^{\frac{(1-\alpha)nF(E-E°)}{RT}} \right) \quad (4)$$

Figure 6 depicts a general pathway for an electrode reaction. The simplest electrochemical reactions involve mass transfer of analyte to the electrode (a), electron transfer between electrode and analyte (b) and mass transfer of the product to the bulk solution (c).[17] Any of these steps could be the rate-limiting step.

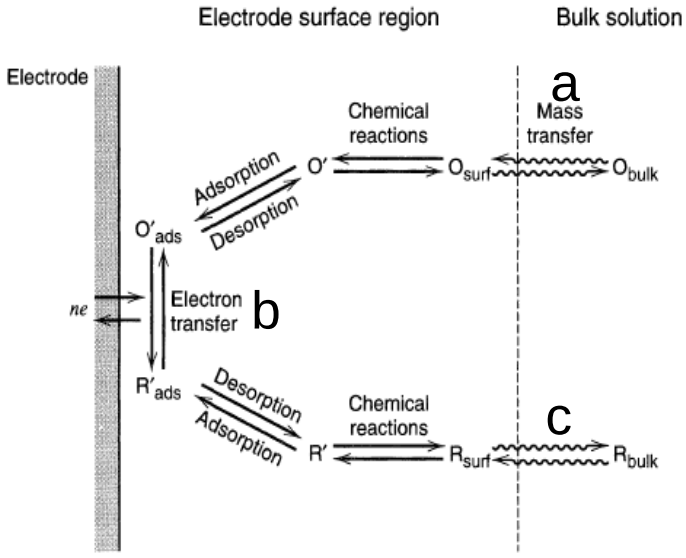

Figure 6. Pathway of a common electrode reaction. Steps a, b and c describe the simplest pathway an electrochemical reaction can have. Modified from Bard, A. J.; Faulkner, L. R. *Electrochemical Methods Fundamentals and Applications*, 2nd ed.; John Wiley & Sons, 2001.

2.3.4 Electrochemical techniques

Electroanalytical measurements can be divided into two categories: potentiometric and potentiostatic.[16,17] Potentiometry measures a potential across an interface with zero current passing through the system. Potentiostatic techniques, also known as controlled-potential techniques, measure the current or resistance that results from a charge transfer process caused by modulating the potential of an electrode. All the techniques discussed in this thesis are potentiostatic.

2.3.4.1 Cyclic voltammetry using macroelectrodes

Cyclic voltammetry is a powerful electroanalytical technique that provides insight into the kinetics and thermodynamics of a redox reaction.[18] To generate a cyclic voltammogram (CV), a potential is linearly swept forward and then backwards and a current vs. potential (i-E curve) is recorded. The potential sweeps have a triangular waveform (Figure 7A) and can be thought of as an excitation signal for the redox reaction. The slope of the waveforms is the scan rate. A CV depicts the current generated at the working electrode as a function of the potential vs. the reference applied to the working electrode.

A typical CV is shown on Figure 7B, obtained by dipping an Au disk electrode in a stagnant 1 mM FcMeOH solution with 0.1 M KCl as the supporting electrolyte and applying the waveform on Figure 7A. At the chosen initial potential of E_i= 0 V, there is not sufficient driving force to initiate FcMeOH oxidation. The potential is scanned positively from 0 V to 0.5 V in the forward sweep. When the potential at the working electrode is positive enough relative to $E^{0'}$, the working electrode accepts electrons from FcMeOH molecules in its vicinity to yield $FcMeOH^+$, generating an anodic current beggining at ~0.15 V. The anodic current reaches a maximum at (b) and begins to decrease because the electrode surface is depleted of FcMeOH due to its oxidation to $FcMeOH^+$. The potential sweep is reversed at (c), and the working electrode is scanned negatively from 0.5 V

to 0 V. Because the potential is sufficiently positive, anodic current is still observed even after switching the potential.[17,18] As the potential is scanned negatively in the reverse scan, the working electrode donates electrons to reduce $FcMeOH^+$ to FcMeOH, resulting in a cathodic current that peaks at (d), at which point the current decreases because the concentration of $FcMeOH^+$ around the working electrode diminishes. [17,18]

As the reaction proceeds, a chemical potential gradient is established around the working electrode and a diffusion layer is created. The concentration of the electroactive species in the diffusion layer is different than in the bulk solution.[16] The rapid change in anodic and cathodic currents is explained by the logarithmic relationship between E and $\frac{[FcMeOH]}{[FcMeOH^+]}$ given in the Nernst equation.[18] The applied potential controls the ratio of oxidized to reduced species in the immediate vicinity of the electrode, thus controlling the thickness of the diffusion layer.[16]

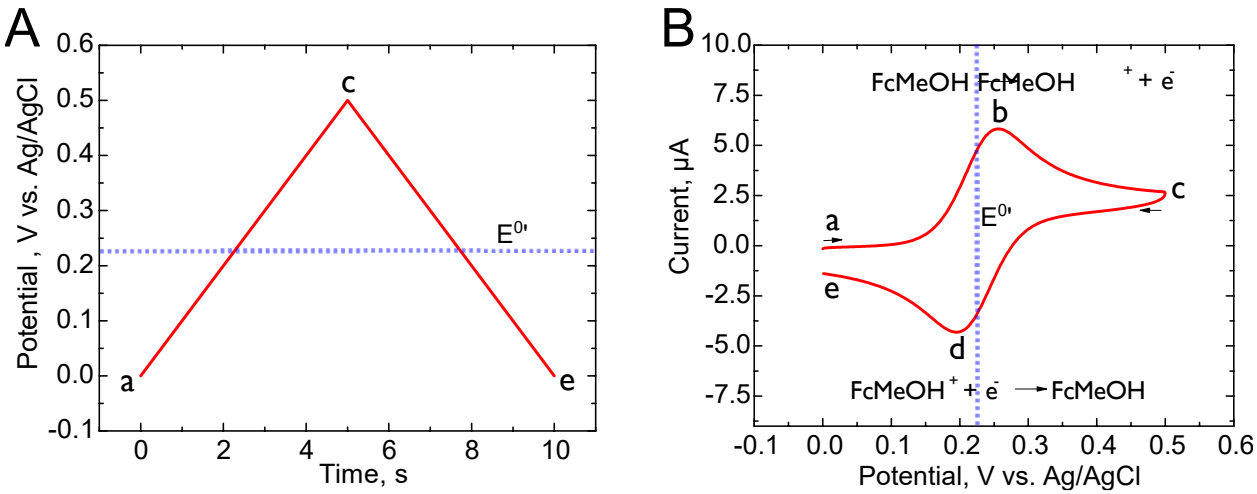

Figure 7. A) Waveform used to generate CV B) Sample CV of a 1 mM FcMeOH, 0.1 M KCl solution, using an Au disk electrode as the working, Ag/AgCl as reference, and a graphite rod as the counter. Dashed line represents E⁰' Arrows indicate direction of each sweep. Modified from Kissinger, P. T.; Lafayette, W.; Heineman, W. R. Cyclic Voltammetry. *J. Chem. Educ.* **1983**, *60* (9), 702–706.

There are four parameters that form the basis for analyzing a CV: the anodic peak current (i_{pa}), the cathodic peak current (i_{pc}), the anodic peak potential (E_{pa}) and the cathodic peak potential (E_{pc}).[16,18] The separation between the peak potentials is given by

$$\Delta E_p = E_{pa} - E_{pc} \approx \frac{0.059\,V}{n} \quad (5)$$

For a reversible, one-electron couple, $\Delta E_p \approx 60$ mV. Quasi-reversible and reversible processes have larger ΔE_p values.

A CV can also offer information on the formal reduction potential ($E^{o\prime}$) of the electroactive species.[18] $E^{o\prime}$ is defined as

$$E^{0\prime} = \frac{E_{pa} + E_{pc}}{2} \quad (6)$$

The Randles-Sevcik equation relates peak current (i_p) to the number of electrons transferred on a redox reaction (n), electrode area (A), diffusion coefficient of the analyte (D), analyte concentration (C) and scan rate (v). It only holds true when the redox process is reversible or quasi-reversible and for semi-infinite linear diffusion. Linearity between peak current and the square-root of the scan rate is typical of a mass transport-limited reaction.

$$i_p = 268{,}600 n^{2/3} A D^{1/2} C v^{1/2} \quad (7)$$

When only the forward scan is collected, the resulting graph is called a linear sweep voltammogram (LSV).[16]

2.3.4.2 Cyclic voltammetry using ultramicroelectrodes

Ultramicroelectrodes (UMEs) are electrodes that have dimensions smaller than 10 μm.[16] As the size of a planar electrode decreases, the diffusional mass-transport in a stagnant solution in the presence of a supporting electrolyte changes from planar to hemispherical. At sufficiently slow scan rates, the shape of the CV will be sigmoidal instead of peak-shaped (Figure 8). A sigmoidal

CV has a limiting current (a) instead of a peak current. The limiting current of a sigmoidal CV (i_{ss}) obtained with a planar disk electrode is given by

$$i_{ss} = 4nFDCr \tag{8}$$

where n is the number of electrons, F is Faraday's constant, D and C are the diffusion coefficient and the concentration of the electroactive species, respectively, and r is the radius of the electrode.

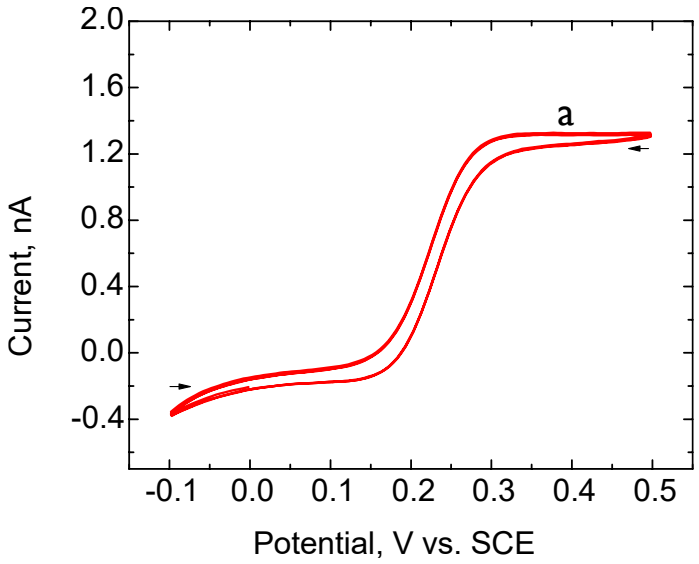

Figure 8. CV of 1 mM FcMeOH at 100 mV s^{-1} generated using a Pt UME as the working and SCE as reference. Arrows indicate direction of each sweep

2.3.4.3 Controlled-potential amperometry

In controlled-potential amperometry, a fixed potential is applied and a current vs. time (i-t curve) is generated.[17] Provided that all charge passed is used to oxidize/reduce the analyte, the area under the i-t curve represents the total number of coulombs consumed and is proportional to the amount of substance electrolyzed. This technique can also be used to electrodeposit a metal on an electrode.

2.4 Semiconductor electrochemistry

Semiconductors have electrical properties between that of a metal and an insulator due to their unique electronic configuration.[17]

2.4.1 Band theory

Band theory describes the electrical properties of solids by considering the molecular orbital structure of bulk materials.[17] The electrons of a single atom occupy orbitals with varying energies, but they also have access to unoccupied orbitals. When the atoms are bonded to other atoms, molecular orbitals are formed by mixing each atom's orbitals of similar energies, creating bonding (lower energy) and antibonding (higher energy) orbitals. In solid materials there are approximately $5x10^{22}$ atoms/cm^3, and the molecular orbitals are so numerous and so closely-spaced that they give rise to bands. The empty antibonding lowest unoccupied molecular orbitals are termed the conduction band (E_C), whereas the filled bonding highest occupied molecular orbitals are termed the valence band (E_V).

The valence and the conduction band can overlap or be separated by forbidden energy levels, where there is very little probability of finding an electron, known as the band gap (E_g).[17] Materials can be classified into three categories depending on their band structures. In conductors, the valence and conducting bands either overlap or are separated by a very small band gap ($E_g << kT$). At virtually any temperature, electrons can readily access the conduction band (or are present there due to overlapping). Under the influence of an electrical field, electrons will then be free to move in the lattice. For insulators, the band gap is large enough ($E_g > 1.5$ eV) to prevent most electrons from accessing the conduction band due to thermal excitation. The electrons have nowhere to go when an electrical field is applied, as the valence band is almost full, and the conduction band is energetically distant. For semiconductors, the band gap allows for some

electrons to jump from the valence band to the conduction band at room temperature. When this occurs, a hole remains in the valence band. Both the electron and the hole have electrical mobility and are referred to as carriers. Electrons can freely move in the vacant conduction band, whereas holes "move" in the valence band by electrons moving to fill the vacancy and leaving behind a hole.

Intrinsic semiconductors, such as Si, are pure materials where the number of holes and electrons are equal.[17] In contrast, an extrinsic semiconductor possesses dopant atoms and an uneven number of carriers, since additional electrons or holes are introduced by the dopant. A donor atom will provide an electron, whereas an acceptor atom provides a hole. Introducing atoms from a group V element, such as N, into Si (a group IV element) adds extra electrons to the conduction band and produces an energy level below the conduction band. These types of materials are known as n-type semiconductors and have electrons as their majority carrier, whereas holes are the minority carriers. Conversely, adding B, a group III element, to Si introduces extra holes on the valence band an energy level above the valence band. B-doped Si is known as a p-type semiconductor, and holes are its majority carrier.

The Fermi level (E_F) is the energy level where the probability is 50% that a level is occupied by an electron.[17] To make it easier to relate E_F of a semiconductor to that of a solution, it can also be described as the electrochemical potential of an electron in a phase and is indicative of the average energy of available electrons. For an intrinsic semiconductor, E_F is found in the bandgap, equidistant from the top of the valence band and the bottom of the conduction band. An n-type semiconductor has its Fermi level closer to the conduction band than the valence band, as doping introduces extra electrons.

2.4.2 Semiconductor-solution junctions

In a solution, the Fermi level is related to the electrochemical potentials of the reduced and oxidized electroactive species.[17] When an inert semiconductor is in contact with a solution and both are at electrostatic equilibrium, the Fermi level of the semiconductor is equal to the Fermi level of the solution.[17,19] By extension, the electrochemical potentials are the same, and so are the average energies of transferable electrons[17,19] Equilibrium is achieved by transferring charge between the phases, as the phase with the highest Fermi level will donate electrons to the phase with the lowest Fermi level until both levels are equal. [17,19]

For example, an n-type semiconductor in contact with a solution reaches equilibrium by donating electrons to the solution until both Fermi levels are identical.[17,19] This causes the semiconductor to possess a positive excess charge, which is distributed in a space-charge region, also known as a depletion region.[17,19] This gives rise to an electric field that affects the electrochemical potential of the semiconductor's electrons, causing the band energies in the space-charge region to differ from those in the field free region of the semiconductor (Figure 9).[17] The band energies bend upward to offset the positive charge in the space-charge region.[17] As the distance from the space-charge region increases, the band energies become more negative until they flatten, since there is no excess charge creating an electric field.[17,19] The potential at which this occurs is known as the flat-band potential (E_{fb}).[17,19]

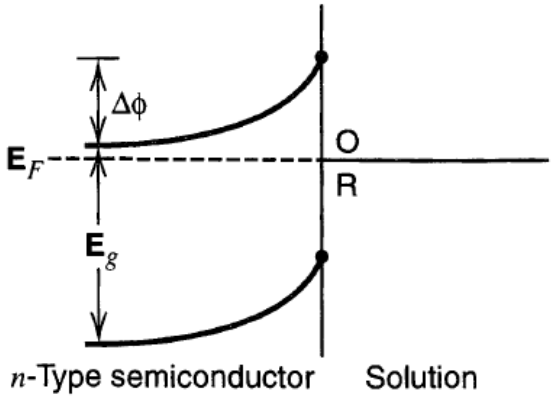

Figure 9. N-type semiconductor/solution junction after equilibration. Taken from Bard, A. J.; Faulkner, L. R. *Electrochemical Methods Fundamentals and Applications*, 2nd ed.; John Wiley & Sons, 2001.

The Mott-Schottky equation relates the capacitance of the space charge region (C_{SC}) to the potential of an electrode versus a reference (E), flat-band potential (E_{fb}), dielectric constant of the semiconductor (ε) and donor density (N_D).[17] At 298 K, it becomes

$$\frac{1}{C_{SC}^2} = \frac{1.41\times10^{20}}{\varepsilon\, N_D}\,(E\ - E_{fb} - 0.0257) \tag{9}$$

The intercept at the potential axis of a $1/C_{SC}^2$ vs. potential plot represents E_{fb}.[17]

2.4.3 Metal-semiconductor junctions

Band-bending also occurs when a semiconductor is in contact with a metal.[17] As in a semiconductor/solution junction, the Fermi levels equilibrate by charge transfer between the metal and the semiconductor.[20] An n-type semiconductor donates electrons to the conduction band of the metal, creating an electron-depleted layer in the semiconductor.[20] After equilibrium is reached, the n-type semiconductor possesses a positive charge, while the metal has a negative charge (Figure 10B). The positive charge in the depletion layer causes an electric field, which gives rise to band-bending.

The barrier height of a metal-n-type semiconductor junction ($q\phi_{Bn0}$) is shown in Figure 10B and is defined as the difference between the Fermi level and the interfacial conduction band edge.[20] For a p-type semiconductor, $q\phi_{Bp0}$ is the difference between the Fermi level and the interfacial valence band edge. When surface states and lattice defects are ignored, the barrier height is equal the difference between the metal work function ($q\phi_m$, the difference between a metal's vacuum level and Fermi level) and the semiconductor's electron affinity ($q\chi$). In reality, the barrier height is highly dependent on factors such as surface contamination and surface states. Consequently, this model does not agree with experimental data. Nevertheless, this simplified version is enough for the purposes of this thesis.

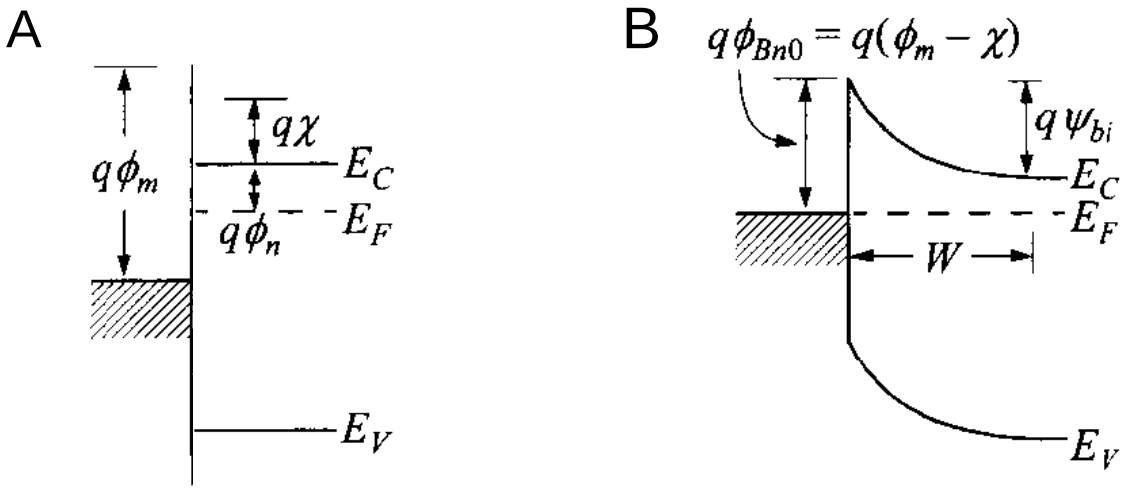

Figure 10. Metal/semiconductor junction before (A) and after (B) equilibration. Taken from S**.** M. Sze, K. K. N. *Physics of Semiconductor Devices*, 3rd ed.; John Wiley & Sons, 2007.

A metal-semiconductor junction with a high barrier height will be rectifying i.e. allows for current flow in a single direction.[20] High-barrier metal-semiconductor junctions are termed Schottky barriers.

2.4.4 Ohmic contacts

Metal-semiconductor contacts with negligible junction resistances are known as ohmic contacts, and are formed when the metal-semiconductor junction has very low Schottky barrier heights.[20] Ohmic contacts' non-rectifying qualities makes them a crucial component of semiconductor devices, as they serve as the connection to the circuit. Ohmic contacts tend to have low barrier heights, so electrons can flow from the semiconductor to the metal and vice versa.

2.4.5 Semiconductor behavior in the dark

In the absence of light, redox processes for a semiconductor in contact with a solution that has energy levels in the bandgap occur through the majority carrier.[17] For example, an n-type semiconductor can only reduce the electroactive species in solution because there are few holes to accept electrons.

When an n-type semiconductor is subjected to potentials more positive than E_{fb}, the carrier concentration at the interface (n_{SC}) is lower than the donor density and the semiconductor is said to be in depletion.[17] When the potential is more positive than E_{fb}, an accumulation layer is formed by electrons gathering in the surface of the semiconductor. The increase in surface carrier concentration makes the semiconductor degenerate, that is, behaving like a conductor.

2.4.6 Semiconductor behavior under illumination

As mentioned earlier, when a semiconductor is in contact with a solution, it will exchange charge with the solution until both Fermi levels are equal, creating a space charge region.[17,19] For an n-type semiconductor, the space-charge region has a positive charge. The absorption of a photon with wavelength > E_g creates an electron-hole pair by promoting an electron to the conduction band and leaving behind a hole in the valence band. Electron-hole pairs that are not in the space

charge region tend to recombine.[17] However, those generated in the space charge region tend to remain separate, as the electric field causes the electrons to migrate away from the space charge region and the holes to migrate towards the semiconductor/solution interface. The holes in the surface have the same effective potential than the valance band edge and thus the semiconductor can cause the electroactive species in solution to oxidize, generating a photoanodic current. The photoassisted oxidation of an electroactive species occurs at more negative applied potentials than those required by an inert metal electrode to perform the same process. Photoeffects typically occur for redox couples with thermodynamic formal potentials more positive than E_{FB}. The thermodynamic formal potential ($E^{0'}$) for a redox couple is found by using an inert metal electrode.

3 Methods and Materials

3.1 Materials and solutions

Ferrocene methanol (FcMeOH; 97%) was obtained from Acros Organics. Calcium chloride ($CaCl_2$), potassium chloride (KCl), potassium nitrate (KNO_3), magnesium chloride hexahydrate ($MgCl_2•6H_2O$), monopotassium phosphate (KH_2PO_4), disodium phosphate (Na_2HPO_4), and monosodium phosphate (NaH_2PO_4) were from Fisher Scientific. Hydrogen tetrachloroaurate(III) trihydrate ($HAuCl_4•H_2O$; 99.99%) was obtained from Alfa Aesar. All chemicals were used as received. To aid in dissolution, FcMeOH solutions were sonicated for 60 minutes and filtered before use. Phosphate-buffered saline (PBS) was prepared by making a 137 mM NaCl, 2.7 mM KCl, 10 Mm Na_2HPO_4 AND 1.8 mM KH_2PO_4 solution. All solutions were prepared using 18.2 MΩ•cm water (Millipore Simplicity).

3.2 Electrode preparation

The electrodes were fabricated using single-side polished, 500-550 µm n-type Si <100> and degenerate (highly doped) p*-Si from WRS wafers. To prepare the electrode, the back of a ~2.25 cm^2 piece of Si is scratched using a diamond scribe in order to remove the native oxide layer. In is soldered on the back to create an ohmic contact and a Cu wire is attached. A circular opening with a 4 mm diameter is made on 3M Electroplater's tape and the tape is used to seal the electrode. This prevents Cu and In from interacting with the solution and to ensure a consistent electrode area.

A modified version of the procedure described by Allongue et al. was used to electrodeposit the Au layer (Figure 11).[21] The electrode is etched in 40% NH_4F solution for 10 minutes to remove the native oxide layer, rinsed and then Au nanoparticles are electrodeposited for 20 minutes under a potential of -1.9 V vs. Ag/AgCl. Electrodeposition is performed using a three-electrode set up,

with Ag/AgCl as the reference and a graphite rod as the counter. In order to prevent an oxide layer from forming, the electrode is biased previous to being dipped in the deposition solution. The deposition solution consists of 1 mM KCl, 0.1 M K_2SO_4 and 1 mM H_2SO_4 and 0.1 mM $HAuCl_4$. All glassware is cleaned in 5% HNO_3 before electrodeposition.

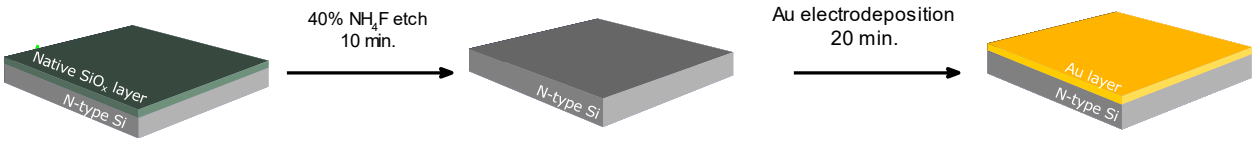

Figure 11. Schematic for the preparation of n-Si|Au photoelectrode.

3.3 Electrochemical characterization

All electrochemical experiments are conducted using a three-electrode arrangement with either Ag/AgCl or saturated calomel electrode (SCE) serving as the reference electrode and Pt or a graphite rod as the counter. The electrodes are tested under three illumination conditions: dark, local illumination and total illumination. For total illumination, either a CH Instruments 660C or 760E potentiostat is used with a 446 mW cm^{-2} white light LED (AM Scope). For local illumination, experiments are performed using a HEKA ELP 1 scanning electrochemical workstation equipped with a PG 160 USB bipotentiostat and a 530-nm LED coupled to a 200-µm fiber optic cable. Dark measurements were performed using a custom-built dark Faraday cage.

3.4 Physical characterization

SEM and EDS images were obtained using a Hitachi S-3400N SEM in secondary electron mode using a 25-kV accelerator voltage.

4 Results and Discussion

In our photoelectrodes, the underlying Si layer is protected with electrodeposited Au nanoparticles. The electrodes are fabricated using a two-step method and characterized in catechol, dopamine and ferrocene methanol using three illumination conditions (Total illumination, local illumination and no illumination). Briefly, we prepare a n-type Si electrode and remove the native SiO_x layer by etching in 40% NH_4F and then electrodeposit Au nanoparticles for 20 minutes.

4.1 Physical characterization

SEM images of the Au layer deposited on n-Si revealed that the surface is covered by Au nanoparticles (Figure 12a). ImageJ was used to determine particle size and coverage. Au NPs covered 33% of the surface and had a diameter of 63 ± 15 nm. EDX analysis confirmed that the electrode surface is mostly Au and Si (Figure 12c).

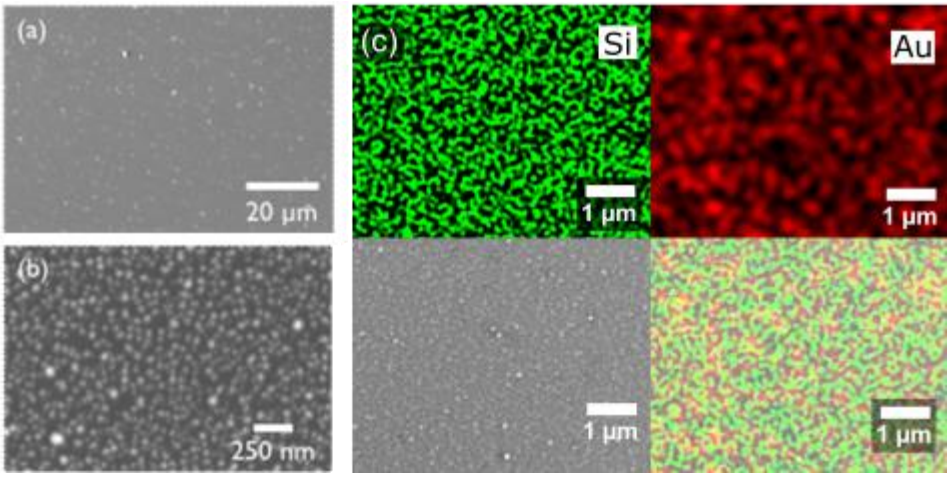

Figure 12. (a) and (b)SEM image of n-Si|Au photoelectrode after Au electrodeposition. (c) EDS map of n-Si|Au photoelecrode after Au electrodeposition

4.2 Total illumination

4.2.1 Electrochemical characterization

Electrodes were tested in 1 mM FcMeOH using total illumination and no illumination. FcMeOH was chosen because it is a well-characterized fast outer-sphere couple. The solutions were not stirred and 0.1 KCl was used as a background electrolyte to ensure diffusion was the principal mode of mass transport.

Figure 13A shows a clear difference between CVs obtained using an n-Si|Au electrode under no illumination (black trace) and total illumination (red trace). Dark currents are two orders of magnitude lower than total illumination currents. When no light is present, the semiconductor layer is in depletion and there are not enough carriers to carry out a redox process. Upon illumination (red trace), enough carriers are generated to make the semiconductor layer degenerate, so a redox reaction is observed. The peak separation (ΔE_p = 61 mV) indicates a reversible process, i.e. fast electron transfer between the analyte and the electrode.

The metallic Si|Au samples were prepared in the same manner as the photoelectrode, but we used p*-type Si (degenerate p-type Si) instead of n-type Si. Due to high doping levels, p*-type Si behaves like a metal, so there is no photoactivity. There was fast electron transfer kinetics between the Au layer in a metallic Si electrode (blue trace) and FcMeOH.

Linearity between the anodic peak current versus the square-root of scan rate confirms that the reaction between FcMeOH and the electrode is mass transport limited, which is crucial for an electrochemical sensor (Figure 13B). Coupled with the reversible ΔE_p value, the results suggest that photon absorption and carrier separation happen rapidly and are not a rate-determining steps.

We determined the flat band potential of the electrode to be -0.061 ± 0.008 V by using Mott-Schottky analysis (Figure 13C). In order to observe a redox reaction between our n-Si|Au

photoelectrode and a redox couple, the thermodynamic formal potential of the redox couple must be more positive than E_{FB}.[17] This is in agreement with our results, as the $E^{0'}$ of the FcMeOH CV taken with a metallic Si|Au electrode in Figure 13A (blue trace) is more positive than the E_{FB} value.

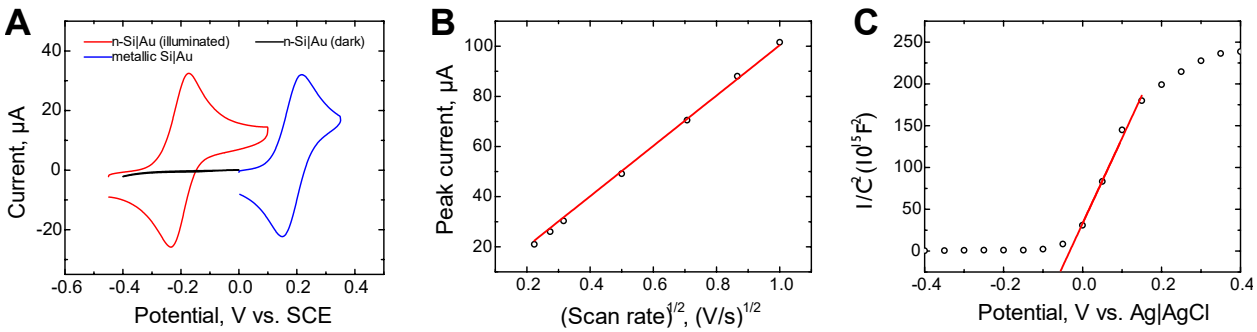

Figure 13. (A) CVs of 1mM FcMeOH, 0.1 M KCl solution using n-Si photo electrode under illumination (red trace), in the dark (black trace) and metallic Si|Au electrode (blue trace). Scan rate= 100 mV/s. (B) Randles-Sevcik analysis of anodic peak current vs square-root of the scan rate. (C) Mott-Schottky plot, x-intercept represents E_{FB} vs. Ag/AgCl.

4.2.2 Stability

The robustness of the photoelectrode was tested by obtaining 1,000 consecutive CVs under total illumination conditions. There was no significant change in the peak separation (ΔE_p=84 mV for all cycles), which indicates that the kinetics of the reaction remained constant (Figure 14A). However, we observed a total positive shift of 0.060 V in $E^{0'}$ between the first and last cycle. We speculate that this was caused by the formation of SiO_x between the Au NPs and the Si layer. Switzer et al. observed the growth of a SiO_x layer in similarly prepared electrodes when they were testing the stability of the electrode in aqueous solution.[22] Since our NP surface coverage is ~33%, some of the Si is exposed to aqueous solution, allowing for lateral undergrowth of SiO_x.[22] Despite the voltage shift, all CVs had the same current values at potentials more positive than -0.05 V vs SCE. If we were to conduct an experiment at a fixed potential, as is the case in many electroanalytical techniques, the shift in $E^{0'}$ becomes less problematic, as currents are similar for potentials above -0.05 V vs SCE. Figure 14A shows that there was a peak current decrease of 12%

between the first and the last CV. As per the Randles-Sevcik equation, the decrease on anodic peak current could have been caused by either degradation of the electrode surface or a change in the concentration of FcMeOH. Since FcMeOH absorbs in the visible range, it is possible that under constant irradiation the solution could have degraded.

To test if the peak current decrease was due to FcMeOH degradation, we repeated the experiment using two metallic Si|Au samples and tested one in the dark and one using total illumination. The sample tested in the dark had exceptional robustness. Peak current and peak separation remained virtually unchanged between cycles 5 and 1000 (Figure 14B). Figure 14C shows a 10% decrease in peak current when the electrolyte was illuminated during the experiment, which we assumed to be caused by FcMeOH degradation, but the peak separation remained constant (ΔE_p= 81 mV for all cycles). These experiments show that the decrease in anodic peak current observed in our n-Si|Au photoelectrode after 1000 cycles was most likely due to both degradation of the FcMeOH solution and the electrode surface.

We wanted to investigate the role that Au NPs play in increasing the robustness of the electrode and improving electron transfer kinetics. Si reacts spontaneously with water to form a passivating layer of SiO_x and the electrodeposited Au NPs help protect Si from being in direct contact with aqueous solution. An n-type Si electrode was prepared and the native SiO_x was etched but did no Au NPs were electrodeposited. Immediately after etching, we tested the electrode using total illumination conditions. A positive total potential shift of 0.147 V in $E^{0'}$ was observed between the first and las cycles, probably caused by the formation of SiO_x (Figure 14D). The peak current decreased by 33%. The electron transfer kinetics became slower with each consecutive CV, as evidenced by the increasing peak separation. Cycle 1 had ΔE_p= 204 mV, whereas cycle 1000 had

ΔE_p= 708 mV. The Au NP coverage improves the electron-transfer kinetics and the durability of the photoelectrode.

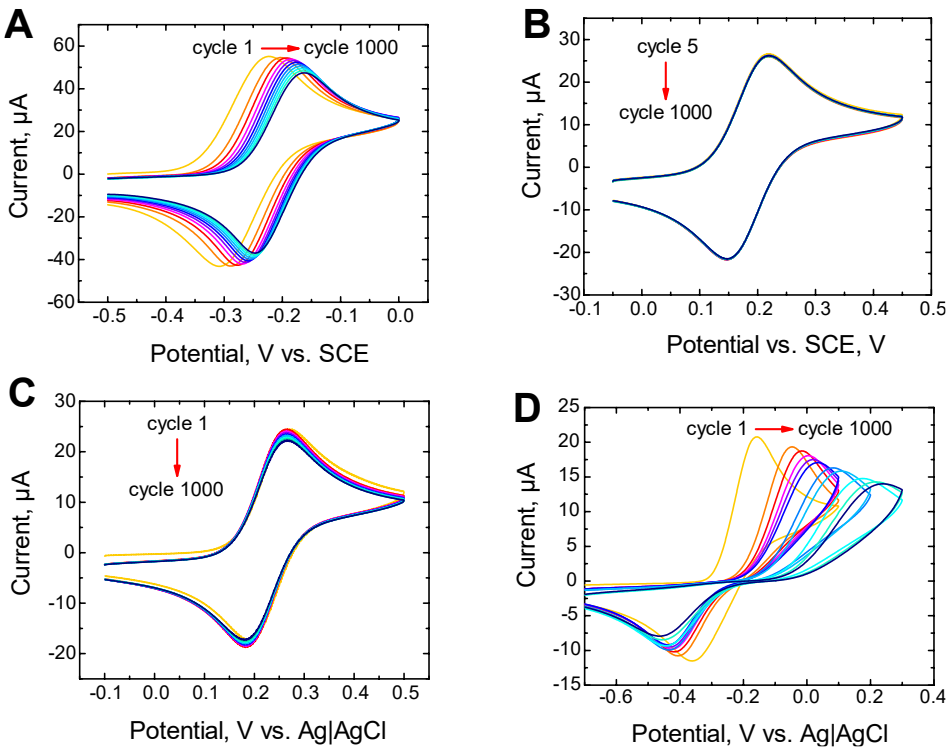

Figure 14. 1000 consecutive CVs at 100 mV s^{-1} scan rate of (A) n-Si photoelectrode, metallic Si|Au (A) in the dark and (B) under illumination, and (D) bare n-type Si. A 2 mM, 0.1 M KCl FcMeOH solution was used for A, all other CVs were obtained using 1 mM FcMeOH, 0.1 M KCl. Counter electrode was a graphite rod for all CVs

4.3 Catecholamine characterization

4.3.1 Catechol

Catechol was chosen for preliminary testing because it possesses the same basic redox structure as catecholamine neurotransmitters.[10] To isolate diffusion as the principal mode of mass-transport, all catechol solutions were stagnant and PBS was used as the background electrolyte. PBS is a commonly used buffer for biological systems.

As expected, we were only able to see the redox process when the n-Si|Au photoelectrode was illuminated, as light is necessary to generate enough carriers to perform the redox reaction. The thermodynamic $E^{0'}$ value is more positive than the E_{FB} (Figure 15A, blue trace).

Catechol oxidation is more complex than FcMeOH oxidation, as it is a 2 e^-/2 H^+ process.[10] It requires the breaking of 2 O-H bonds and the creation of two C-O bonds, so an intramolecular reorganization energy barrier needs to be overcome in order to perform the reaction, resulting in sluggish electron transfer kinetics.[16] Moreover, neurotransmitter oxidation is typically an inner-sphere reaction, which contributes to slow electron-transfer kinetics.[23] This explains the irreversible behavior (ΔE_p = 281 mV) observed when a CV was obtained using catechol as the analyte (Figure 15A, red and blue traces). Despite the slow kinetics, we obtained a calibration curve by illuminating a n-Si|Au electrode, obtaining CVs of 30 µm-1 mM dopamine solutions and plotting the current at E=0 V vs. dopamine concentration (Figure 15B and 15C). The linearity of the calibration curve was excellent (R^2=0.991) and the photoelectrode had a sensitivity of m=(3.05±0.08) x10^{-8} A/µM. The LOD (= $3\sigma_{blank}$/m) was 3.4 µM.

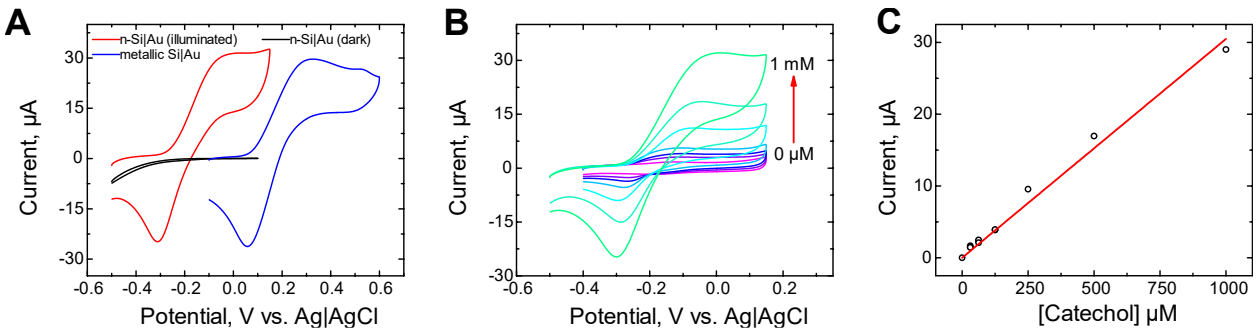

Figure 15. (A) CVs of 1mM catechol in PBS buffer at 100 mV s^{-1} scan rate using n-Si|Au photoelectrode under illumination (red trace), in the dark (black trace) and metallic Si|Ay electrode (blue trace). (B) CVs of catechol at different concentrations collected under total illumination using n-Si|Au photoelectrode at scan rate 100 mV s^{-1}. (C) Catechol calibration curve. R^2= 0.991

4.3.2 Dopamine

Illumination of the photoelectrode is necessary to observe significant dopamine oxidation, as light is necessary for the generation of carriers (Figure 16A, black and red traces). The dopamine CV obtained by using a metallic Si|Au electrode has a $E^{0'}$ more positive than the E_{FB}, which is consistent with what we would expect (Figure 16A, blue trace). The sluggish electron-transfer

kinetics (ΔE_p= 123 mV, Figure 16A) are caused by the complex inner-sphere $2H^+/2e^-$ process that is necessary to oxidize dopamine.[16,23]

Dopamine calibration curves obtained by illuminating the n-Si|Au photoelectrode and plotting peak current vs. dopamine concentration possessed excellent linearity (R^2=0.992), which is an encouraging result (Figure 16B and 16C). The sensitivity of the calibration curve, (6.2 ± 0.3) x10^{-8} A μM^{-1}, is three orders of magnitude larger than those reported by Chung et. al. (1.29 x 10^{-11} – 5.64 x10^{-11} A μM^{-1}).[15] Our LOD was 9 µM, which is higher than those reported by Chung et. al. (0.597-0.670 µM). Our high LOD is due to high background currents.

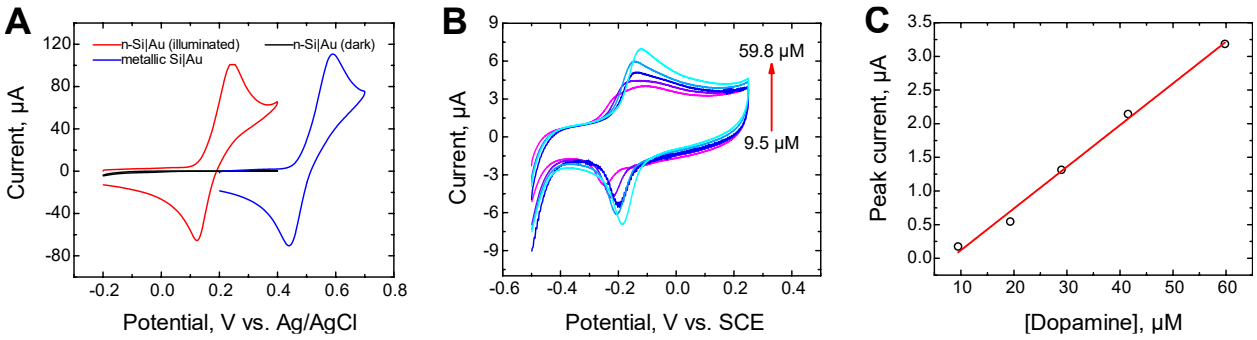

Figure 16. (A) CVs of 1mM dopamine, 1 mM $HClO_4$ in PBS buffer at 100 mV s^{-1} scan rate using n-Si photo electrode under total illumination (red trace), in the dark (black trace) and metallic Si|Au electrode (blue trace). (B) CVs of dopamine in PBS buffer at different concentrations collected using nSi photoelectrode. (C) Dopamine calibration curve. R^2= 0.992

It was noted that the electrode degraded when repetitive dopamine runs where performed, even at low dopamine concentrations. Dopamine is known to foul electrodes by forming polydopamine, an insulating polymer that adsorbs onto the electrode surface.[23] However, since the fouling only occurs where the electrode is illuminated, we could overcome this hurdle by moving to a different spot on the electrode.

4.4 Local illumination

The photoelectrode was maintained at a potential of 0.1 V vs. Ag/AgCl and an i-t curve was generated while employing a light with a 200 μm diameter. The light-source was turned on/off for 10 seconds, and the cycle was repeated for one hour. Fig 17A shows that the current spikes immediately after illumination. When the light was turned off, the current sharply decreased to zero. The fast response of the electrode to the light stimulus suggests the possibility of making measurements with high temporal resolution. Moreover, the electrode was stable for one hour of continuous testing.

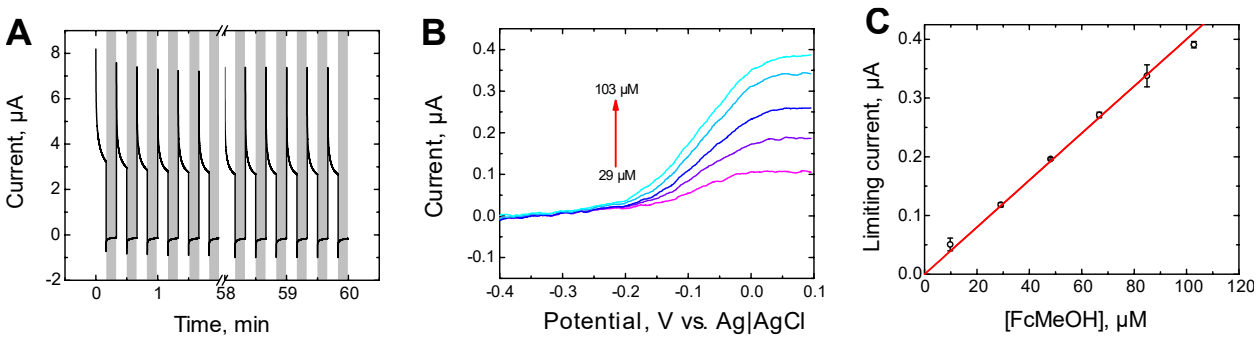

Figure 17. (A) Chopped light i-t curve of photoelectrode in 2 mM FcMeOH, 0.1 M KCl. Shaded region represents when the light was off. (B) LSVs of FcMeOH at different concentrations collected using n-Si|Au photoelectrode at scan rate 100 mV s^{-1}. (C) Dopamine calibration curve. R^2= 0.991. All experiments used Ag/AgCl as a reference electrode and Pt wire as the counter.

The LSVs used for the calibration curve did not have the expected peak shape. We predicted a peak-shaped LSV based on the diameter of the light source, but the LSVs have vaguely sigmoidal shapes with higher currents than we anticipated. For a 200 μm electrode in contact with a 100 μM FcMeOH solution, the Randles-Sevcik equation predicts an anodic peak value of ~7 nA. The predicted limiting current for an electrode in identical conditions is 3 nA. Our currents are ~2 orders of magnitude larger than those predicted by both equations. However, if we use the observed limiting current to calculate the electrode diameter using Randles-Sevcik, the diameter is 1.4 mm,

roughly 1.4 times smaller than the actual area of the electrode. These suggests that we were able to decrease the active electrode area by only illuminating a fraction of the surface.

A possible explanation for the high currents is the high values in the minority carrier diffusion distance in crystalline n-type Si, which is on the order of 100-300 μm. It is possible for carriers to be generated at the site of local illumination but travel 100-300 μm before the redox event takes place, making our active surface larger than the illuminated portion. It is also possible that our illuminated area is higher than 200 μm because the light that exits the fiber optic cable is not collimated. However, these do not fully account for the high observed currents.

Although we observed excellent linearity (R^2 = 0.998) when a calibration curve using FcMeOH was attempted in this set up, we cannot confidently say we are limited by mass-transport, as there is much we do not understand about our local illumination experiments (Figure 17C).

5 Conclusions

Light-addressable electrodes could potentially solve some of the drawbacks of traditional electrode arrays and electrochemical imaging techniques by providing high spatiotemporal resolution. Although a very exciting prospect, there are not many examples in the literature about light-addressable electrodes. This thesis describes the fabrication and characterization of light-addressable electrodes for neurotransmitter sensing. We fabricate the electrodes in a simple two-step process by depositing Au NPs on n-type Si and physically characterize them using SEM. The electrochemical characterization is done in a three-electrode arrangement and three different illumination conditions (total illumination, local illumination and no illumination), using FcMeOH, catechol and dopamine as the analytes.

The photoelectrodes were only able to pass significant current when illuminated, regardless of what redox active species was used (FcMeOH, catechol and dopamine). Light served as a "switch" to turn the electrochemical reaction on or off. When the whole electrode surface was illuminated (total illumination) and $FcMeOH/FcMeOH^+$ was used as a redox couple, the reaction had fast electron-transfer kinetics and was mass-transport limited, as evidenced by the peak separation (61 mV) and the linearity between anodic peak current and the square-root of the scan rate, respectively. Our photoelectrode was stable after 1000 CVs, and the current remained constant at potentials higher than -0.05V.

Slower electron-transfer kinetics were observed when the photoelectrodes were challenged with dopamine and catechol. Oxidation of both of these electroactive species is considerably more complex than FcMeOH oxidation, as they involve the transfer of $2\ e^-/\ 2H^+$. Regardless, dopamine and catechol calibration curves have excellent linearity (R^2=0.991 and 0.992, respectively).

Local illumination experiments showed that we are able to reduce the active electrode surface when just a fraction of the total electrode was illuminated. The temporal resolution under these conditions was promising. We are also able to obtain a FcMeOH calibration curve with excellent linearity (R^2=0.998).

Despite these encouraging results, there is much we do not understand about our local illumination experiments. The shape of our curves is not what we expected, and the currents were higher than those predicted by Randles-Sevcik and UME limiting current. We also need to assess how light intensity affects our observed currents. This is of capital importance, as the photocurrent is controlled by light intensity in addition to analyte concentration.[15,19,24] Recently, Esposito et. al. investigated the parameters that switched H^+ reduction in a flow reactor from being mass transport-limited to being light-limited.[24] Knowing the conditions that make our local illumination system limited by mass-transport is essential to confidently measure analyte concentration.

To be desirable for *in vitro* imaging, dopamine sensors need to have high selectivity for dopamine in the presence of many other similar molecules.[11] We did not measure dopamine in the presence of epinephrine or norepinephrine, which are present in the extracellular matrix of neurons.[11] All catecholamines have similar E^0 values, which difficult selectivity when using electrochemical techniques.[10] In addition, our LOD is too big, as a dopamine sensor must be able to detect dopamine concentrations on the nM range. Our large LOD is mainly due to our large background signal. The background signal could be reduced by employing a different electrochemical technique, such as amperometry or square-wave voltammetry.

Although we mainly focused on dopamine sensing, we believe our electrodes could be suitable for other applications such as very high measurement density and imaging. The main obstacle that needs to be overcome in order to achieve this is the low spatial resolution caused by

the high minority carrier diffusion distance (100-300 μm) of the crystalline n-type Si. Recently, the Gooding group used a layer of amorphous silicon on FTO to decrease the carrier diffusion distance, which is an approach we would like to take in the future.[25]

6 References

(1) Choudhury, M. H.; Ciampi, S.; Yang, Y.; Tavallaie, R.; Zhu, Y.; Zarei, L.; Gonçales, V. R.; Gooding, J. J. Connecting Electrodes with Light: One Wire, Many Electrodes. *Chem. Sci.* **2015**, *6* (12), 6769–6776. https://doi.org/10.1039/c5sc03011k.

(2) Wang, J.; Trouillon, R.; Dunevall, J.; Ewing, A. G. Spatial Resolution of Single-Cell Exocytosis by Microwell-Based Individually Addressable Thin Film Ultramicroelectrode Arrays. *Anal. Chem.* **2014**, *86* (9), 4515–4520. https://doi.org/10.1021/ac500443q.

(3) Hafez, I.; Kisler, K.; Berberian, K.; Dernick, G.; Valero, V.; Yong, M. G.; Craighead, H. G.; Lindau, M. Electrochemical Imaging of Fusion Pore Openings by Electrochemical Detector Arrays. *Proc. Natl. Acad. Sci.* **2005**, *102* (39), 13879–13884. https://doi.org/10.1073/pnas.0504098102.

(4) Wang, J.; Trouillon, R.; Lin, Y.; Svensson, M. I.; Ewing, A. G. Individually Addressable Thin-Film Ultramicroelectrode Array for Spatial Measurements of Single Vesicle Release. *Anal. Chem.* **2013**, *85* (11), 5600–5608. https://doi.org/10.1021/ac4009385.

(5) Kurulugama, R. T.; Wipf, D. O.; Takacs, S. A.; Pongmayteegul, S.; Garris, P. A.; Baur, J. E. Scanning Electrochemical Microscopy of Model Neurons: Constant Distance Imaging. *Anal. Chem.* **2005**, *77* (4), 1111–1117. https://doi.org/10.1021/ac048571n.

(6) Engstrom, R. C.; Pharr, C. M. Scanning Electrochemical Microscopy. *Anal. Chem.* **1989**, *61* (19), 1099A–1104A. https://doi.org/10.1021/ac00194a002.

(7) Schulte, A.; Nebel, M.; Schuhmann, W. Scanning Electrochemical Microscopy in Neuroscience. *Annu. Rev. Anal. Chem.* **2010**, *3* (1), 299–318. https://doi.org/10.1146/annurev.anchem.111808.073651.

(8) Takahashi, Y.; Shiku, H.; Murata, T.; Yasukawa, T.; Matsue, T. Transfected Single-Cell Imaging by Scanning Electrochemical Optical Microscopy with Shear Force Feedback Regulation. *Anal. Chem.* **2009**, *81* (23), 9674–9681. https://doi.org/10.1021/ac901796r.

(9) Choudhury, M. H.; Ciampi, S.; Lu, X.; Kashi, M. B.; Zhao, C.; Gooding, J. J. Spatially Confined Electrochemical Activity at a Non-Patterned Semiconductor Electrode. *Electrochim. Acta* **2017**, *242*, 240–246. https://doi.org/10.1016/j.electacta.2017.04.177.

(10) Robinson, D. L.; Hermans, A.; Seipel, A. T.; Wightman, R. M. Monitoring Rapid Chemical Communication in the Brain. *Chem. Rev.* **2008**, *108* (7), 2554–2584. https://doi.org/10.1021/cr068081q.

(11) Labib, M.; Sargent, E. H.; Kelley, S. O. Electrochemical Methods for the Analysis of Clinically Relevant Biomolecules. *Chem. Rev.* **2016**, *116* (16), 9001–9090. https://doi.org/10.1021/acs.chemrev.6b00220.

(12) Kashi, M. B.; Silva, S. M.; Yang, Y.; Gonçales, V. R.; Parker, S. G.; Barfidokht, A.; Ciampi, S.; Gooding, J. J. Light-Activated Electrochemistry without Surface-Bound Redox Species. *Electrochim. Acta* **2017**, *251*, 250–255. https://doi.org/10.1016/j.electacta.2017.08.127.

(13) Lian, J.; Yang, Y.; Wang, W.; Parker, S. G.; Gonçales, V. R.; Tilley, D.; Gooding, J. J. Amorphous Silicon on Indium Tin Oxide : A Transparent Electrode for Simultaneous Light Activated Electrochemistry and Optical Microscopy †. *Chem. Commun.* **2019**, 123–126. https://doi.org/10.1039/c8cc07889k.

(14) Yang, Y.; Ciampi, S.; Zhu, Y.; Gooding, J. J. Light-Activated Electrochemistry for the Two-Dimensional Interrogation of Electroactive Regions on a Monolithic Surface with

Dramatically Improved Spatial Resolution. *J. Phys. Chem. C* **2016**, *120* (24), 13032–13038. https://doi.org/10.1021/acs.jpcc.6b02289.

(15) Seo, D.; Lim, S. Y.; Lee, J.; Yun, J.; Chung, T. D. Robust and High Spatial Resolution Light Addressable Electrochemistry Using Hematite (α-Fe 2 O 3) Photoanodes. *ACS Appl. Mater. Interfaces* **2018**, *10* (39), 33662–33668. https://doi.org/10.1021/acsami.8b10812.

(16) Wang, J. *Analytical Electrochemistry*, Second.; Wiley-VCH, 2000.

(17) Bard, A. J.; Faulkner, L. R. *Electrochemical Methods Fundamentals and Applications*, Second.; John Wiley & Sons, 2001.

(18) Kissinger, P. T.; Lafayette, W.; Heineman, W. R. Cyclic Voltammetry. *J. Chem. Educ.* **1983**, *60* (9), 702–706. https://doi.org/10.1021/ed060p702.

(19) Walter, M. G.; Warren, E. L.; McKone, J. R.; Boettcher, S. W.; Mi, Q.; Santori, E. A.; Lewis, N. S. Solar Water Splitting Cells. *Chem. Rev.* **2010**, *110* (11), 6446–6473. https://doi.org/10.1021/cr1002326.

(20) S. M. Sze, K. K. N. *Physics of Semiconductor Devices*, Third.; John Wiley & Sons, 2007.

(21) Prod'Homme, P.; Maroun, F.; Cortès, R.; Allongue, P. Electrochemical Growth of Ultraflat Au(111) Epitaxial Buffer Layers on H-Si(111). *Appl. Phys. Lett.* **2008**, *93* (17), 21–24. https://doi.org/10.1063/1.3006064.

(22) Chen, Q.; Switzer, J. A. Photoelectrochemistry of Ultrathin, Semitransparent, and Catalytic Gold Films Electrodeposited Epitaxially onto n - Silicon (111). *ACS Appl. Mater. Interfaces* **2018**, *10* (111), 21365–21371. https://doi.org/10.1021/acsami.8b06388.

(23) Peltola, E.; Sainio, S.; Holt, K. B.; Paloma, T.; Laurila, T. Electrochemical Fouling of Dopamine and Recovery of Carbon Electrodes. *Anal. Chem.* **2018**. https://doi.org/10.1021/acs.analchem.7b04793.

(24) Davis, J. T.; Esposito, D. V. Limiting Photocurrent Analysis of a Wide Channel Photoelectrochemical Flow Reactor. *J. Phys. D. Appl. Phys.* **2017**, *50* (8). https://doi.org/10.1088/1361-6463/aa5538.

(25) Vogel, Y. B.; Gonçales, V. R.; Gooding, J. J.; Ciampi, S. Electrochemical Microscopy Based on Spatial Light Modulators: A Projection System to Spatially Address Electrochemical Reactions at Semiconductors. *J. Electrochem. Soc.* **2018**, *165* (4), H3085–H3092. https://doi.org/10.1149/2.0111804jes.